Available online at www.sciencedirect.com
SCIENCE DIRECT®
PERGAMON
International Journal of Heat and Mass Transfer 46 (2003) 3221–3231
International Journal of HEAT and MASS TRANSFER
www.elsevier.com/locate/ijhmt

# Simulation and experiment of the unsteady heat transport in the onset time of nucleation and crystallization of ice from the subcooled solution

Frank G.F. Qin [a,*], Jian Chao Zhao [a], Andrew B. Russell [a,1], Xiao Dong Chen [a], John J. Chen [a], Lindsay Robertson [b]

[a] *Department of Chemical and Materials Engineering, The University of Auckland, Private Bag 92019, Auckland, New Zealand*

[b] *Fonterra Research Centre, Palmerston North, New Zealand*

Received 30 August 2002; received in revised form 31 January 2003

**Abstract**

Heat transfer is an unsteady process in the initial period of ice nucleation or phase transition from aqueous solution. During this period the latent heat of freezing increases the temperature in bulk solution monotonously until the system reaches equilibrium. Meanwhile heat can transfer from the solution to the environment or vise versa. The analysis of this unsteady heat transfer process leads to the establishment of a mathematical model, which is represented by two simultaneous differential equations. Using the *Laplace* transform and inverse transform, and incorporating the initial condition of ice nucleation, we obtained an analytical solution of this model. Further discussion of the model's fitness by comparing to the experimental data leads to a recognition that ice fouling (or ice adhesion) on the cooler wall should be highlighted in estimating the heat transfer resistance at the very beginning of the ice formation. The model fits to the experimental data satisfactorily.


*Keywords:* Unsteady heat transfer; Nucleation; Ice formation; Freeze concentration; *Laplace* transform

## 1. Introduction

Phenomena of the onset of ice nucleation and crystallization from the subcooled solution have been studied by many researchers. One of the basic motives, in early years, was the requirement of freeze concentration (or freeze desalination), in which the solution was concentrated as the result of ice crystallization (and the ice itself was desalinated). A general problem is the tendency of forming very fine ice crystals so that the separation of the final concentrate from the ice slurry becomes difficult. Incomplete separation of ice and liquid leads to the loss of valuable solute.

The phenomena of ice formation and nucleation aroused new interest in recent years because of the consideration of using ice–aqueous-solutions as heat (or cold) storage system. For this purpose, Intemann and Kazmierczak did experimental researches on the heat transfer and ice formations deposited upon subcooled tube banks immersed in flowing water [1,2]. In their paper, the increasing heat transfer resistance of the ice scales was recognized and emphasized during the phase change process. To prevent the ice adhesion on the cooling surface, Tsuchida et al. used stainless steel with PFA (tetra-fluro-ethylene-perfluoro-alkylvinyl-ether-copolymer) resin coating and PTFE (poly-tera-fluoro-ethylene) as the cooling surface, and employed an emulsion, which was a mixture of silanol–aqueous solution and silicone oil, as the heat storage material [3].

* Corresponding author.
*E-mail address:* fqin001@ec.auckland.ac.nz (F.G.F. Qin).
[1] Current address: Unilever R&D Coluworth, Sharnbrook Bedford, UK.

0017-9310/03/$ - see front matter 
doi:10.1016/S0017-9310(03)00097-8

**Nomenclature**

| | |
|---|---|
| $A_s$ | area of the heat transfer surface ($m^2$) |
| $C_{pl}$, $C_{ps}$ | specific heat capacity of the liquid and steel plate respectively ($J\,kg^{-1}\,°C^{-1}$) |
| $h_l$ | the individual heat transfer coefficient of the liquid film when ice fouling dose not exist ($W\,m^{-2}\,°C^{-1}$) |
| $\Delta H_i$ | latent heat of freezing (J/kg) |
| $k_i$ | rate constant of the ice formation ($kg\,s^{-1}\,m^{-3}\,°C^{-1}$) |
| $K_{ls}$ | overall heat transfer coefficient between the liquid (whole milk in this study) and the steel ($1/K_{ls} = (1/h_l) + (L_s/\lambda_s)$) ($W\,m^{-2}\,°C^{-1}$) |
| $L_s$ | thickness of the steel plate (m) |
| $T_s$ | temperature of the cooler surface (°C) |
| $T_c$ | temperature of the coolant (°C) |
| $T_l$ | temperature of the solution at an arbitrary time (°C) |
| $T_f$ | freezing point of the solution (°C) |
| $V_l$, $V_s$ | volumes of the liquid and steel plate ($m^3$) |

*Greek symbols*

| | |
|---|---|
| $\rho_l$, $\rho_s$ | density of the liquid and the steel ($kg\,m^{-3}$) |
| $\lambda_s$ | thermal conductivity of the steel ($J\,m^{-1}\,°C^{-1}$) |
| $\delta_i$ | the thickness of the ice layer formed on the cooler surface as the result of ice fouling (m) |
| $\theta$ | dimensionless temperature, $\theta_l = (T_l - T_{l0})/(T_f - T_{l0})$ and $\theta_s = (T_s - T_{s0})/(T_f - T_{l0})$ |
| $\zeta$ | weight content of liquid in ice layer |

They found that the slurry ice could be formed without adhesion to the cooling surface if the heat flux of the wall was less than a critical value.

In the case of scale formation of ice on subcooled solid surfaces, in which there is no nucleation from bulk solutions, the unsteady heat transfer with phase-change moving boundary is often formulated as the classical Stefan problem [4]. Numerical solutions were also developed to extend the application to solid, multicomponent moisture-containing system. For example, freezing of foodstuffs (meat, fruit, etc.), and formation of frozen soil are among the interesting applications [5–7].

In the process of freeze concentration, the behaviors of ice nucleation and crystallization greatly determine the size distribution of ice crystals. Therefore a comprehensive understanding of the kinetics of nucleation and crystallization of ice will benefit the design of process and equipment, as well as the optimization of the operation.

To study the kinetics of secondary nucleation and crystallization of ice, an ordinary method is to count the number of nuclei and to measure the size (or mass) of crystals formed [8,9]. This method proved to be tedious and time consuming, even though high-tech sophisticated instrument, such as the particle analyzer, could be used for nuclei counting and size analysis [10]. In contrast to this, a much easier approach, the thermal response method, was developed by Kane [11], and was modified by researchers, like Kane et al. [12], Omran and King [13], Stocking and King [14], and Shirai et al. [15,16].

In a low supercooling degree, when ONE tiny ice crystal is introduced into the water or solution, it will initiate a secondary nucleation, which will be followed by ice crystallization. The temperature response curve would have a typical profile as shown in Fig. 1 [11].

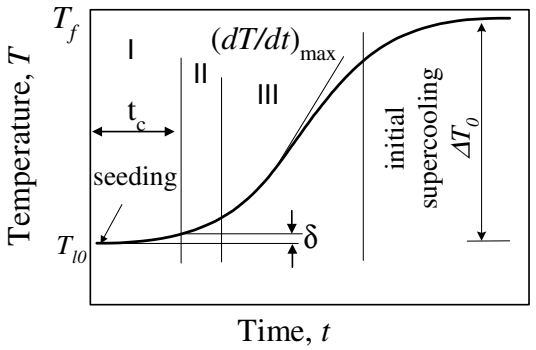


Fig. 1. Thermal response curve ($T_f$ is the freezing point of the solution, which is the equilibrium temperature when time ($t$) is large enough).

By assuming that the growth rate $\dot{R}$ is proportional to the instantaneous supercooling $S(= T_f - T)$ and inversely proportional to the radius $R$ of the ice particle according to experimental observation, namely

$$\dot{R} = \frac{gS}{R} \tag{1}$$

Omran and King derived a model to obtain the nucleation and crystallization parameters from the thermal response curve that can be measured by experiment:

$$\delta = \frac{4\sqrt{2}\cdot \Delta H_i \rho_i k_v b g^{1.5} (\Delta T_0)^{i+1.5} t_c^{2.5}}{5MC_p} \tag{2}$$

where $\delta$ is the temperature increase of the bulk ($\delta = T - T_{l0}$), compared to the temperature at the seeding time; $\Delta H_i$ is the latent heat of freezing; $\rho_i$, the density of the ice; $k_v$, the volume shape factor; $b$, the nucleation rate constant including the effect of the seed

characteristics, flow conditions, etc.; $g$, the growth rate factor representing the dependency of the diffusivity and the thermal conductivity of the solution, flow conditions, etc.; $\Delta T_0$, the initial supercooling ($\Delta T_0 = T_f - T_{l0}$); $t_c$, the time interval (or termed as induction time); $M$, the total mass in the crystallizer; and $C_p$ the specific heat capacity of the contents of crystallizer.

However if growth rate $\dot{R}$ is assumed to be proportional to the $m$th power of supercooling $S$ (where $m \neq 1$), which is independent to the radius $R$ of the ice particle, rather than inversely proportional to it (Eq. (1)), namely

$$\dot{R} = g \cdot S^m \tag{3}$$

another thermal response equation (4) could be obtained:

$$\delta = \frac{4\sqrt{2} \cdot \Delta H_i \rho_i k_v b (g')^3 (\Delta T_0)^{i+3m} t_c^4}{4MC_p} \tag{4}$$

Definitions of the symbols in Eq. (4) are the same with those in Eq. (1). The powers of $t_c$ in Eqs. (2) and (4) are different because of different assumptions of the growth kinetics between Eqs. (1) and (3). Plotting $\ln \delta$ versus $\ln(t_c)$ with the experimental data, Omran and King found that curves keep in straight lines in the slope of 2.5, this verified that the postulation for Eq. (1) is correct, i.e. the growth rate is proportional to the instantaneous supercooling but inversely proportional to the radius of ice. However, as $\delta$ increases, for example when $\delta$ is larger than 0.1 °C, the curves deviate from straight lines. This means that only when the values of $\delta$ are very small, e.g. smaller than 0.1 °C, is the Eq. (2) valid. The interpretation of this, according to Omran and King [12], is that during the induction time $t_c$, nucleation rate is dominated by the ice seed (note only one tiny ice seed is added). The first batch of newborn secondary nuclei is all induced by one ice particle, and they are still too small to induce the next generation of secondary nuclei. After this period when the first batch of nuclei grows big enough to induce the next generation of secondary nucleation, the model is inapplicable. The value of $\delta$ is so small that a very high-resolution thermal probe (e.g. 0.0001 °C) is required. This is an obstacle to use the thermal response method to extract the kinetics parameter of nucleation and crystallization. Moreover Eq. (2) indicates that the increase of the induction time ($t_c$) measured leads to the decrease of the nucleation rate or growth rate of ice crystals. However these cannot be evaluated independently.

Based on the proposal of Kane et al. for the case of size dependent growth [12], Shirai et al. extended the method to calculate the temperature response curve and the change in crystal size distribution during batch crystallization [15]. The maximum slope and the kinetic parameter $\beta$ was given by the following equation:

$$\beta^0 \Delta T = 5.93 (\mu_2^0)^{0.027} \left( \frac{dT}{dt} \right)_{mas} \tag{5}$$

where $\mu_2^0$ is the initial second moment of crystal size distribution, and $\beta^0$, the initial value of $\beta$. The kinetic parameter $\beta$ corresponds to the nucleation rate per crystal particle in a continuous crystallizer and depends on the nucleation rate and the growth rate of ice crystals [12].

Experiments used to verify the models mentioned above were all conducted in small volume vessels, for instance, no more than 400 ml, and in very small initial supercooling conditions, for instance, less than 0.2 °C. In contrast with these, Chen and Chen [17] used large volume of liquid solution running through a helical tube which was submerged in deep subfreezing coolant. The interval time from the beginning of the liquid entering the tube to the moment that nuclei appeared at the outlet of the tube was defined as the 'induction time'. The ice induction times were correlated with the kinetic parameters with a sublayer reactor model:

$$\frac{dn_0}{dt} = A_{rfo} e^{-\frac{E}{RT}} (n_0)^m \tag{6}$$

where $n_0$ is the nuclei concentration in the fluid near metal surface ($m^{-3}$); $T$ is the temperature (K); $E$ is the apparent activation energy of the process ($J\,mol^{-1}$); $A_{rfo}$ is the apparent frequency factor ($s^{-1}$); $R$ is the universal gas constant ($= 8.31\ J\,mol^{-1}\,K^{-1}$). $m$ is a constant.

The apparent activation energy of nucleation was calculated through numerical computation.

$$E \approx 1076.85 \times 10^3 \Delta T^{-1.67}\ (kJ\,mol^{-1}) \tag{7}$$

where $\Delta T$ is the supercooling (K).

## 2. Experimental

The equipment used in this study was a 2.5-liter suspension crystallizer. The experimental setup is shown in Fig. 2. The bulk temperature was controlled by the cooling jacket at the bottom. A HAAKE 20A unit (Gebruder HAAKE GmbH, Germany) provided and recycled the coolant for the jacket. The temperature of the coolant could be preset to a desire value in an accuracy of ±0.05 °C. Flow bafflers were used in the jacket cooler to eliminate stagnant regions. Temperatures of the bulk solution, metal surface, coolant inlet and outlet were measured with a set of K-type thermocouples, and were recorded via a Picolog TC-08 (Pico Technology Ltd., Hardwick, UK) in a computer. Agitation was employed by a gear-driven motor (KIKA works Sdn. Bhd., Malaysia; 60–600 rpm) via a 4-straight-blade impeller (6.5 cm diameter and 1.5 cm high), which is preset to 100 rpm in this study. The experimental system was thermal insulated wherever appropriate.

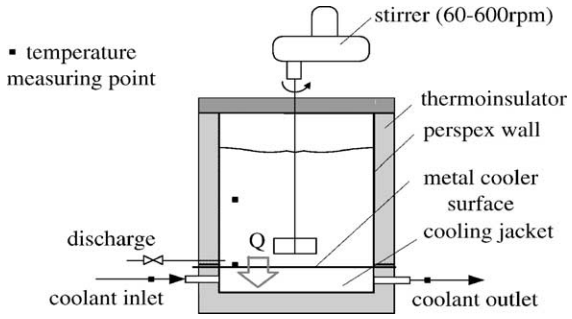


Fig. 2. Schematic diagram of the crystallizer.

The bulk temperature was gradually decreased at a rate of 0.2 °C min$^{-1}$ by programming the HAAKE 20A unit properly. When the bulk temperature reached a certain critical temperature, spontaneous nucleation would take place. Fig. 3 shows a thermal response curve of ice spontaneous nucleation form whole milk at the wall temperature of −4.67 °C.

Phase transition can also be triggered by introducing the ice seeds into the subcooled aqueous solution before the solution reaches to the critical temperature. Fig. 4 shows a thermal response curve where ice formation started after the addition of a small ice particle.

The experimental observation to the onset period of the nucleation of ice showed that the following steps occurred in this unsteady process:

(1) Under the condition of the agitation, after the onset of spontaneous nucleation, a large amount of the ice crystals are quickly formed in the solution.
(2) At the moment of onset time of nucleation (or seeding), the thermal response curve, i.e., the temperature–time curve, had a singularity (see Figs. 3 and 4). The bulk temperature and the wall temperature increased with time due to the release of the latent heat of ice formation until the system approached to the thermal equilibrium.
(3) The heat was also partially transferred through the steel plate to the coolant. This caused an increase in the temperature of the steel plate. However, the temperature of the coolant is assumed unchanged due to sufficient supply of coolant.

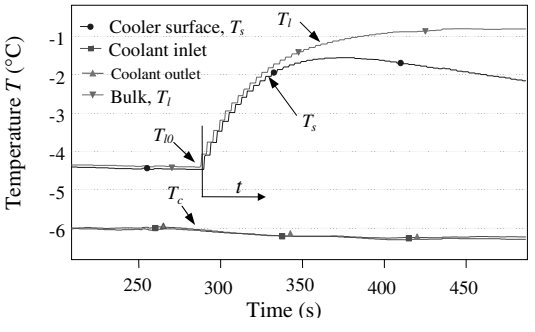


Fig. 3. Spontaneous nucleation in whole milk (10 wt%).

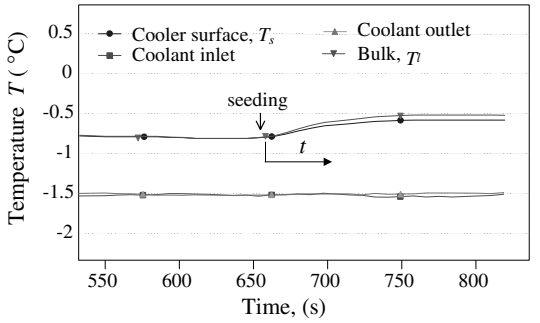


Fig. 4. The thermal response curve of secondary nucleation of ice in whole milk triggered by seeding the milk with an ice particle.

The profile of temperature $T_l$ varying with time, $t$, conjectured by intuition, is similar to the process of charging a capacitance. In other word, it behaves like a first-order system [18]. A parallel analogy between the solution temperature, $T_l$ and voltage of a capacitance gives a following guess:

$$T_l = T_{l0} + \Delta T \cdot (1 - e^{-st}) \tag{8}$$

where $T_{l0}$ is the initial temperature of the bulk when nucleation takes place; $\Delta T$, the initial supercooling which is $T_f - T_{l0}$; $t$ the time elapse after nucleation (or seeding), and $s$ a time constant which is similar with the constant of $1/RC$ in the *resistance–capacitance* circuit. So Eq. (8) can also be written as

$$\frac{T_l - T_{l0}}{T_f - T_{l0}} = 1 - e^{-st} \tag{9}$$

However, this expression is not obtained from any serious mathematical derivation. Further analysis is required to establish a more comprehensive mathematical model for the unsteady heat transfer process during the onset time of ice formation in a homogenous solution.

## 3. Modeling

### 3.1. Assumptions and derivation of the model

In order to simplify the mathematical analysis. The process was modeled based on the following assumptions:

(1) During process of ice formation, the physical properties of the solution, such as the specific heat capacity, the volume and the density keep unchanged.
(2) Temperatures of the inlet and outlet coolant do not change with time during the process of ice formation

because of the flow rate of coolant is sufficient enough to withdraw the heat flux which passes through the jacket wall.

(3) The rate equation of the ice formation is assumed to be the first order, i.e., $dm_i/dt = k_i \cdot (T_f - T_l)$ where $m_i$ is the ice mass formed per volume of the solution ($kg\,m^{-3}$); $k_i$ is the rate constant ($kg\,m^{-3}\,s^{-1}\,°C^{-1}$), which was recognized to be independent with the temperature in the limited range of supercooling, e.g. $T_f - T_l < 3$ °C [13]; $T_f$ is the freezing point of the solution, and $T_l$ is the instantaneous temperature of the solution.

(4) The heat transfer resistance is attributed to (a) the liquid film on the cooler surface, and (b) the metal wall of the cooling jacket.

(5) The thermal insulation on the exterior of the vessel is sufficient, so the heat loss is negligible.

(6) Since the thickness of the steel plate is small and there is no heat source inside it, the gradient of the temperature across the steel plate is assumed to be linear. Thus, the average temperature of the steel plate will be the average of the "hotter" surface temperature $T_s$, which is the cooler surface temperature, and the "colder" surface temperature $T_c$, which is the coolant temperature.

Based on the experimental observation and the assumptions made above, the following heat balances can be recognized:

Balance I: Heat accumulation in the bulk = latent heat of ice formation – heat transferred to the steel plate; and

Balance II: Heat accumulation in the steel plate = heat transferred into the steel from the bulk – heat transferred out of the steel into the coolant.

Therefore, the following simultaneous differential equations are established based on balances I and II, as well as the initial conditions of Eq. (12):

$$C_{pl}V_l\rho_l \cdot \frac{dT_l}{dt} = \Delta H_i \cdot k_i \cdot V_l \cdot (T_f - T_l) - h_l \cdot A_s \cdot (T_l - T_s) \tag{10}$$

$$\frac{C_{ps}V_s\rho_s}{2} \cdot \frac{dT_s}{dt} = h_l \cdot A_s \cdot (T_l - T_s) - \frac{\lambda_s}{L_s} \cdot A_s \cdot (T_s - T_c) \tag{11}$$

$$T_s|_{t=0} = T_{s0},\ T_l|_{t=0} = T_{l0} \tag{12}$$

Definitions and the significance of the symbols used in these equations are listed in the Nomenclature.

In Eq. (11), the average temperature of the steel plate is $(T_s)_{av} \approx (T_s + T_c)/2$, and the coolant temperature was a constant (i.e. $dT_c/dt = 0$), so $d(T_s)_{av}/dt = dT_s/2dt$. Therefore the left-hand side of Eq. (11) becomes $C_{ps}V_s\rho_s/2 \cdot dT_s/dt = C_{ps}V_s\rho_s(d(T_s)_{av}/dt)$, which represents the heat accumulation in the steel plate. $T_s$ and $T_l$ represent the cooler surface (on the liquid side) and the bulk temperatures, respectively. They are variables. All the others are constants. Eq. (12) denotes the initial condition of the ice formation from the subcooled solution.

Introduce the dimensionless temperature:

$$\theta_l = \frac{T_l - T_{l0}}{T_f - T_{l0}}$$

and

$$\theta_s = \frac{T_s - T_{s0}}{T_f - T_{l0}}$$

Eqs. (10)–(12) become:

$$\frac{d\theta_l}{dt} = \frac{\Delta H_i \cdot k_i}{C_{pl}\rho_l} \cdot (1 - \theta_l) - \frac{h_l \cdot A_s}{C_{pl}V_l\rho_l} \cdot \left(\theta_l - \theta_s + \frac{T_{l0} - T_{s0}}{T_f - T_{l0}}\right) \tag{13}$$

$$\frac{d\theta_s}{dt} = \frac{2h_l \cdot A_s}{C_{ps}V_s\rho_s} \cdot \left(\theta_l - \theta_s + \frac{T_{l0} - T_{s0}}{T_f - T_{l0}}\right) - \frac{2\lambda_s \cdot A_s}{L_sC_{ps}V_s\rho_s} \cdot \left(\theta_s + \frac{T_{s0} - T_c}{T_f - T_{l0}}\right) \tag{14}$$

$$\theta_s|_{t=0} = 0, \quad \theta_l|_{t=0} = 0 \tag{15}$$

Using the *Laplace* transform and applying the initial conditions, then performing the inverse *Laplace* transform, we obtain the analytical expression of the dimensionless temperature $\theta_l$:

$$\theta_l = f_0 + f_1 \exp(-s_1 t) - f_2 \exp(-s_2 t) \tag{16}$$

Derivation of this solution is detailed in the Appendix A of this paper. Here in Eq. (16), $f_0$, $f_1$ and $f_2$ as well as $s_1$ and $s_2$ are constants. Their definitions and calculations are also detailed in Appendix A. Another analytical solution $\theta_s$ is regarding the temperature profile inside the steel plate of the jacket. Since its thickness is thin whilst it has a relatively high thermal conductivity, the temperature distribution can be treated as linear. So the analytical solution $\theta_s$ was not presented in this paper.

According to initial condition, when $t = 0$, we have

$$\theta_l|_{t=0} = f_0 + f_1 - f_2 = f_0 + \frac{f_0 \cdot s_2 - k_2}{s_1 - s_2} - \frac{f_0 \cdot s_1 - k_2}{s_1 - s_2} \equiv 0 \tag{17}$$

when time tends to infinity, Eq. (16) gives

$$\theta_l|_{t\to\infty} = f_0 = 1 - \left[\frac{T_f - T_{l0}}{T_f - T_c} + \frac{\Delta H_i V_l k_i (T_f - T_{l0})}{K_{ls}A_s(T_f - T_c)}\right]^{-1} \tag{18}$$

The second term in right-hand side of Eq. (18) is generally very small, for example, it is 0.027948 in the case of this study. The factor

$$\frac{\Delta H_i V_l k_i \cdot (T_f - T_{l0})}{K_{ls}A_s \cdot (T_f - T_c)}$$

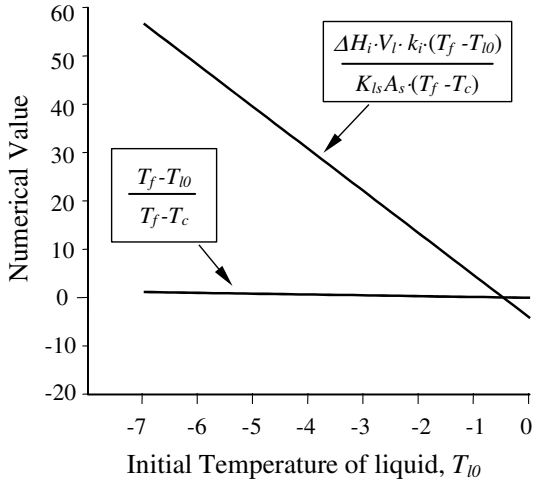


Fig. 5. Variation of $(T_f - T_{l0})/(T_f - T_c)$ and $(\Delta H_i V_l k_i (T_f - T_{l0}))/(K A_s (T_f - T_c))$ with the initial temperature $T_{l0}$.

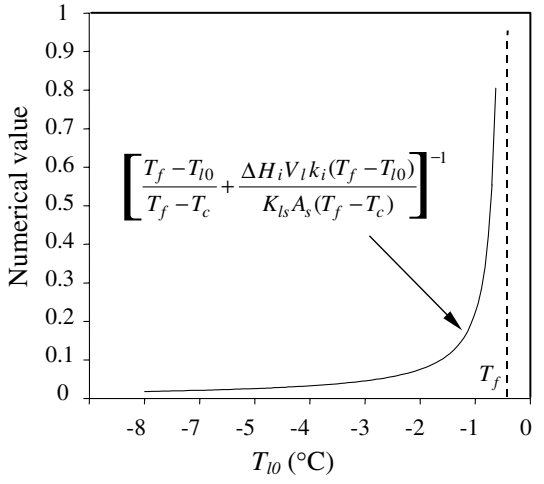


Fig. 6. When $T_{l0}$ approaches to freezing point $T_f$, $[(T_f - T_{l0})/(T_f - T_c) + (\Delta H_i V_l k_i (T_f - T_{l0}))/(K_{ls} A_s (T_f - T_c))]^{-1}$ is infinite.

denotes the ratio of the heat generation rate in the bulk to the heat transportation rate out of the bulk. $(T_f - T_{l0})/(T_f - T_c)$ expresses the initial condition of the system, which is always larger than zero and smaller than one. When the initial supercooling of the liquid $(\Delta T_0 = T_f - T_{l0})$ is larger than a certain value, e.g. $\Delta T_0 > 0.2$ °C, the heat generation rate is normally overwhelming, but the heat transfer rate is limited (see Fig. 5). This results in that the value of $f_0$ is very close to 1.

There is a pseudo-singularity in Eq. (18) when the initial temperature of the liquid $T_{l0}$ approaches the freezing point of the liquid $T_f$, both

$$\frac{T_f - T_{l0}}{T_f - T_c}$$

and

$$\frac{\Delta H_i V_l k_i (T_f - T_{l0})}{K_{ls} A_s (T_f - T_c)}$$

approach to zero, leading to infinity of the second term of Eq. (18), as shown in Fig. 6. However, the definition of the dimensionless temperature is $\theta_l = (T_l - T_{l0})/(T_f - T_{l0})$, substituting it into (18) and letting $T_{l0} \to T_f$, Eq. (18) can be rewritten as

$$\left. T_l \right|_{\substack{T_{l0} \to T_f \\ t \to \infty}} = \lim_{\substack{T_{l0} \to T_f \\ t \to \infty}} \left\{ (T_f - T_{l0}) \cdot \left[ 1 - \left( \frac{T_f - T_{l0}}{T_f - T_c} + \frac{\Delta H_i V_l k_i (T_f - T_{l0})}{K_{ls} A_s (T_f - T_c)} \right)^{-1} \right] + T_{l0} \right\}$$

$$= \lim_{t \to \infty} \left( T_f - \frac{K_{ls} A_s (T_f - T_c)}{K_{ls} A_s + \Delta H_i V_l k_i} \right) = T_c \qquad (19)$$

Note the limit "$\lim_{t \to \infty} (\Delta H_i V_l k_i) = 0$" means when $t$ is large enough, the latent heat released by ice formation will end up with all the liquid is frozen ($V_l \to 0$), and the system temperature will finally approach to the coolant temperature $T_c$. Therefore with this expression, the singularity is eliminated.

### 3.2. Comparison of the simulation results with the experimental results

Based on Eq. (16), the analytical solution of the mathematical model, the variation of the dimensionless temperature of the aqueous solution is simulated. The parameter values used in this simulation are listed in Table 1.

The smooth line in Fig. 7 is the simulated result and the broken line is the experimental result, which always locates above the position of the simulated curve indicating that the simulated value is smaller than that of the experimental value. There are two possibilities: (i) Ice formation proceeds in a higher rate than being predicted in the initial time, which release more latent heat to raise temperature in the bulk; or (ii) the heat transfer resistance is actually higher than the value that we estimated based on the assumption (4), where the heat transfer resistance was assumed to consist of two parts: the individual heat transfer coefficient ($h_l$) of the liquid film on the cooler surface, and the thermal conductivity of the steel plate ($\lambda_s$). If the first case is true, the two curves should finally approach to the same value and meet together when crystallization time is long enough and the system approaches to a thermal equilibrium. However, this did not happen in our experiments indicating that the discrepancy of the preliminary model with the

experimental result was likely attributed to the second reason: the heat transfer resistance was underestimated. Then what else has not been considered?

It was probably the ice fouling on the cooler surface, which was the result of ice growth adhering on the subcooled metal surface. In the preliminary model, ice fouling was not considered to be a heat transfer resistance in the very beginning of ice formation. However, since the cooler surface had a lower temperature than that in the bulk, in an well-agitated condition, ice formation and crystallization may probably proceed simultaneously both in the bulk and on the cooler surface as well [19]. Were this true, the heat transfer resistance of this ice layer would quickly dominate the heat transfer rate because of its small thermal conductivity.

However, the initial ice fouling (or ice layer) is not visible even in pure water. Up to now, no data available on the ice layer thickness and the porosity of this layer. This makes it difficult to estimate the individual heat transfer coefficient of the fouling layer.

The overall heat transfer coefficient is therefore modified in the following procedures:

(1) The individual heat transfer coefficient of the liquid film on solid surface remains the same: 266 ($W m^{-2} °C^{-1}$), as listed in Table 1.
(2) The fouling layer of ice is estimated to be 1 mm in average. The thermal conductivity of the ice at 0 °C is 2.26 $W m^{-1} °C^{-1}$.
(3) The content of the liquid in the ice layer is estimated to be 15%(w/w). This value was abstracted from

Table 1
Parameters used in the simulation

| Symbol | Value | Unit |
|---|---|---|
| $A_s$ | $2.269 \times 10^{-2}$ | $m^2$ |
| $\rho_l$ | 1060 | $kg/m^3$ |
| $\rho_s$ | 7900 | $kg/m^3$ |
| $h_l^{(1)}$ | 266 | $W m^{-2} °C$ |
| $\Delta H_i$ | 334110 | J/kg |
| $\lambda_s$ | 15 | $W m^{-1} °C$ |
| $L_s$ | $5.0 \times 10^{-3}$ | m |
| $T_f$ | −0.49 | °C |
| $V_l k_i^{(2)}$ | $8.45 \times 10^{-4}$ | kg/s °C |
| $T_{l0}$ | −4.09 | °C |
| $T_{s0}$ | −4.46 | °C |
| $T_c$ | −6.34 | °C |
| $C_{pl}$ | 3910 | J/kg °C |
| $C_{ps}$ | 502.3 | J/kg °C |
| $V_l$ | $2.20 \times 10^{-3}$ | $m^3$ |
| $V_s$ | $1.134 \times 10^{-4}$ | $m^3$ |
| $A_s$ | $2.269 \times 10^{-2}$ | $m^2$ |

*Note*: (1) $h_l$ is the individual heat transfer coefficient of the liquid film on the cooler surface. It can be expressed as [22].

$$h_l = 0.664 \frac{\lambda_l}{D} Re^{1/2} Pr^{1/3} \tag{20}$$

where $\lambda_l$ is the thermal conductivity of the liquid which is around 0.53 $W m^{-1} °C^{-1}$ for the whole milk at nearby of 0 °C [23,24]. $D$ is the diameter of the tank bottom. $Re$ is the *Reynolds* number in the bulk and $Pr$ is the *Prandtl* number of whole milk. At −0.5 °C it was estimated to be

$$Pr = \frac{c_p \mu}{\lambda_l} = \frac{3.91 \times 10^3 \times 0.005}{0.53} = 36.89,$$

and the stirring *Reynolds* number in the tank was estimated to be

$$Re = \frac{n D_{stir}^2 \rho}{\mu} = \frac{100 \times (6.5 \times 10^{-2})^2 \times 1.06 \times 10^3}{60 \times 0.005} \approx 1493.$$

Therefore the individual heat transfer coefficient of the liquid film can be calculated as

$$h_l = \frac{0.664 \times 0.53 \times (1493)^{1/2} \times (36.89)^{1/3}}{5 \times 10^{-2}} \approx 266 \ W m^{-2} °C^{-1}.$$

(2) Estimated from the best fit for the first 0–49 s.

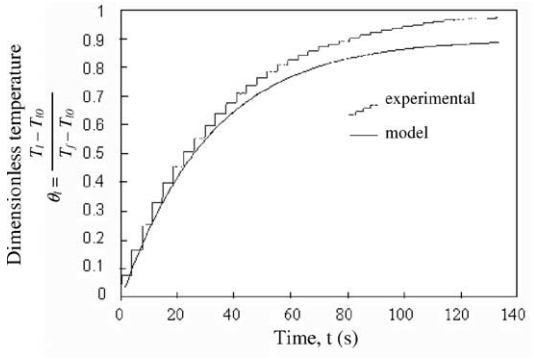


Fig. 7. Comparison of the simulation results to the experimental results without considering the ice fouling on the cooler wall.

Ping Chen's work, who measured the solute concentration of the ice layer fouled on subcooled surface of a heat exchanger [20]. The thermal conductivity of the liquid (i.e. whole milk in this study) at 0 °C is 0.53 $W m^{-1} °C^{-1}$.

(4) The overall heat transfer coefficient between the liquid (whole milk in this study) and the cooler surface is therefore estimated as

$$K_{ls} = \frac{1}{\frac{1}{h_l} + \frac{\delta_i}{\zeta\lambda_l + (1-\zeta)\lambda_{ice}}} = \frac{1}{\frac{1}{266} + \frac{0.001}{0.15\times 0.53 + 0.85\times 2.26}} = 234.8\ (W m^{-2} °C^{-1}) \quad (21)$$

where $\delta_i$ is the thickness of the ice layer formed on the cooler surface, $\lambda_l$ and $\lambda_{ice}$ is the thermal conductivities of liquid and the ice, respectively. $\zeta$ is the liquid content by weight of the ice layer, which is assumed to be 15% (w/w) in this study.

Using $K_{ls} = 234.8$ ($W m^{-2} °C$) to substitute $h_l = 266$ ($W m^{-2} °C$) in simulating the heat transfer with Eq. (16), we can compare the experimental and the simulation results again in Fig. 8.

A comparison between Figs. 7 and 8 shows that there is an obvious improvement after the heat transfer resistance due to the developing ice layer is considered. The best estimation of the heat transfer resistance may be carried out based on the best fit between the experimental data and the simulation equation (16). Using the ice formation (nucleation) in the whole milk (~10% (w/w) solid concentration) as an example again, a further analysis of the analytical solution of the mathematical model, i.e. Eq. (16), shows that in three terms of the right-hand side of the equation, only the first term $f_0$ and the third term $f_2 \exp(-s_2 t)$ make a significant contribution to the dimensionless temperature $\theta_l$, while the second term $f_1 \exp(-s_1 t)$ is always very close to zero (it is $9.6 \times 10^{-4}$ at the beginning and rapidly approaches to zero as the time increase), so that it is negligible. If

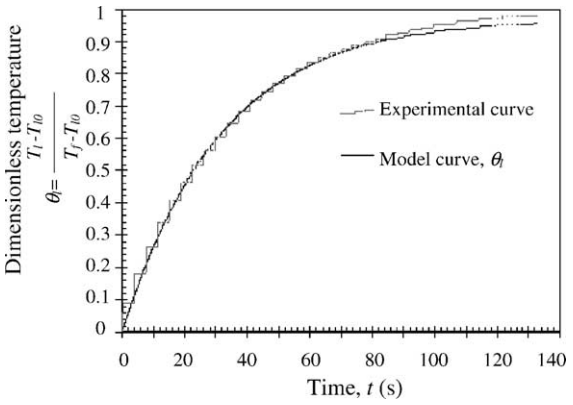


Fig. 8. Comparison of the simulation results to the experimental results. The effect of the ice fouling on the heat transfer had been considered in this simulation.

ignoring the second term $f_1 \exp(-s_1 \cdot t)$, we can obtain a simplified expression of Eq. (16) as following (Fig. 9):

$$\theta_l = f_0 - f_2 \exp(-s_2 t) \quad \text{or}$$

$$\frac{T_l - T_{l0}}{T_f - T_{l0}} = f_0 - f_2 \exp(-s_2 t) \quad (22)$$

As we discussed before the constant $f_0$ is very close to 1, as is $f_2$. An extreme scenario is that during the period of ice formation, the vessel is ideally thermal insulated. There is neither the heat exchange between the liquid and the environment, nor the heat 'leakage' to the coolant. Thus the overall heat transfer coefficient $K_{ls}$ trend to zero, this leads to the following results according to their definitions (Appendix A):

$$f_0|_{K_{ls}\to 0} = 1, \quad f_2|_{K_{ls}\to 0} = 1, \quad \text{and} \quad s_2|_{K_{ls}\to 0} = \frac{\Delta H_i k_i}{C_{pl}\rho_l} \quad (23)$$

Therefore Eq. (22) becomes the same as Eq. (9), expressing an interesting aspect that for an adiabatic nucleation process in a supercooled aqueous solution, the temperature profile would have the same mathematical expression with the voltage profile of a capacitance which is being charged. Moreover, Eq. (9) would have a concrete version as the following:

$$\frac{T_l - T_{l0}}{T_f - T_{l0}} = 1 - \exp\left(-\frac{\Delta H_i k_i}{C_{pl}\rho_l}\cdot t\right) = 1 - \exp\left[-\frac{k_i (T_f - T_{l0})}{\rho_l \cdot S_T}\cdot t\right] \quad (24)$$

where $\Delta H_i$ the latent heat of freezing (kJ/kg), $k_i$ the constant of ice formation rate in the bulk ($kg m^{-3} °C^{-1}$), $C_{pl}$, $\rho_l$, the heat capacity ($kJ m^{-3} °C^{-1}$) and the density ($kg m^{-1}$) of the liquid, respectively. $S_T$ is the *Stephen* number ($S_T = C_{pl}(T_f - T_{l0})/\Delta H_i$), which expresses the ratio of sensible heat to the latent heat of the liquid. Because

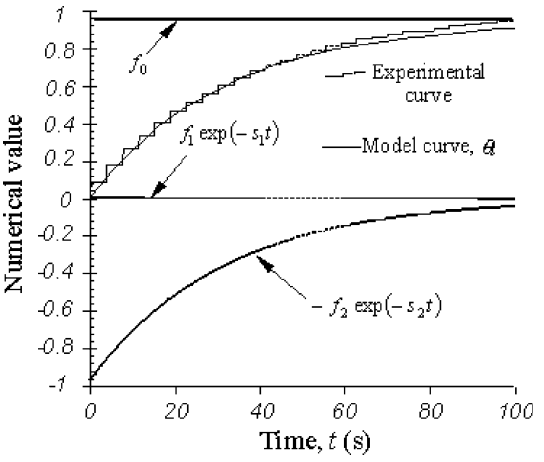


Fig. 9. The individual contribution of the three terms in Eq. (16) to the value of $\theta_l$.

$$\Delta H_i k_i / C_{pl}\rho_l = \frac{\Delta H_i k_i V_l (T_f - T_{l0})}{C_{pl}\rho_l V_l (T_f - T_{l0})}$$

the numerator clearly represents the heat generation rate given by ice formation in the bulk, and the denominator represents the thermal inertia of the liquid. This ratio has the dimension of reciprocal of time. Therefore $C_{pl}\rho_l/\Delta H_i k_i$ is factually the time constant of this first-order linear system.

## 4. Conclusions

In an well-agitated subfreezing aqueous solution with a supercooling larger than 0.2 °C, once the ice formation starts, the thermal response curve would show a singularity at the onset time of phase transition. The phase transition can be triggered by the spontaneous nucleation or by the addition of ice seeds into the solution. However, a smooth thermal response curve, which implicates a lag of the occurrence of ice particles (or 'induction time') after seeding the solution according to the model proposed by Omran and King [14] was not observed in this supercooling region. This can be explained by proposing that when supercooling is larger than a certain value, e.g. $\geqslant 0.2$ °C, the induction time is too short to be properly measured.

The model developed in this study considers that the total ice formation rate is a function of supercooling, and the predominating factor of ice formation rate from dilute aqueous solution is the heat transfer resistance. This proved to be true by the experiments of this study, particularly when the solute concentration of the aqueous phase is under 10% (w/w). In a higher solute concentration, the viscosity of the solution rapidly increases, the diffusion of water molecules to the ice surface (i.e. the mass transfer step) may gradually become important and can not be ignored. In that case, the model will not be applicable.

Theoretically, ice formation rate is the integration result of nucleation rate and the growth rate of all the ice particles. Though previous studies indicated that the nucleation rate of ice in a small supercooling (e.g. <0.2 °C) is the 2.5th power of the supercooling, and the growth rate is inversely proportional to the radius of an individual ice particle [14]. However these can not be used to predict the total ice formation rate.

In the discussion of modifying the preliminary model in the latest section of this paper, we introduced a further assumption that a thin ice layer starts to grow on the cooler surface once the ice formation is initiated in the bulk solution. After incorporating the heat transfer resistance of this ice layer into the model, the model met the experimental results much better, indicating ice fouling followed the ice formation in the bulk almost immediately. This has been confirmed in a more direct way in another experiment of this study, and the issues about in what condition that the ice layer occur, and how long it will need to cover the entire cooler surface were studied and modeled in another paper [21].

## Appendix A

The derivation of the solution of the Eqs. (10) and (11) through *Laplace* transform.

Rewrite Eqs. (13)–(15):

$$\frac{d\theta_l}{dt} = \frac{\Delta H_i \cdot k_i}{C_{pl} V_l} \cdot (1 - \theta_l) - \frac{h_l \cdot A_s}{C_{pl} V_l \rho_l} \cdot \left(\theta_l - \theta_s + \frac{T_{l0} - T_{s0}}{T_f - T_{l0}}\right) \tag{A.1}$$

$$\frac{d\theta_s}{dt} = \frac{2h_l A_s}{C_{ps} V_s \rho_s} \cdot \left(\theta_l - \theta_s + \frac{T_{l0} - T_{s0}}{T_f - T_{l0}}\right) - \frac{2\lambda_s \cdot A_s}{L_s C_{pl} V_s \rho_s} \cdot \left(\theta_s + \frac{T_{s0} - T_c}{T_f - T_{l0}}\right) \tag{A.2}$$

$$\theta_s|_{t=0} = 0, \quad \theta_l|_{t=0} = 0 \tag{A.3}$$

Let

$$A = \frac{\Delta H_i k_i}{C_{pl}\rho_l}; \quad B = \frac{h_l \cdot A_s}{C_{pl} V_l \rho_l};$$

$$C = \frac{h_l \cdot A_s}{C_{pl} V_l \rho_l} \cdot \frac{T_{l0} - T_{s0}}{T_f - T_{l0}} = B \cdot \frac{T_{l0} - T_{s0}}{T_f - T_{l0}};$$

$$D = \frac{2h_l \cdot A_s}{C_{ps} V_s \rho_s}; \quad E = \frac{2h_l \cdot A_s}{C_{ps} V_s \rho_s} \cdot \frac{T_{l0} - T_{s0}}{T_f - T_{l0}} = D \cdot \frac{T_{l0} - T_{s0}}{T_f - T_{l0}};$$

$$F = \frac{2 \cdot \lambda_s \cdot A_s}{L_s C_{ps} V_s \rho_s} \quad \text{and}$$

$$G = \frac{2 \cdot \lambda_s \cdot A_s}{L_s C_{ps} V_s \rho_s} \cdot \frac{T_{s0} - T_c}{T_f - T_{l0}} = F \cdot \frac{T_{s0} - T_c}{T_f - T_{l0}}$$

Eqs. (A.1) and (A.2) can be simplified as

$$\frac{d\theta_l}{dt} + (A+B)\theta_l = B\cdot\theta_s + (A-C) \tag{A.4}$$

$$\frac{d\theta_s}{dt} + (D+F)\theta_s = D\cdot\theta_l + (E-G) \tag{A.5}$$

$$\theta_s|_{t=0} = 0, \quad \theta_l|_{t=0} = 0 \tag{A.6}$$

Take *Laplace* transform for Eqs. (A.4) and (A.5), since $L(d\theta_l/dt) = s\overline{\theta}_l - \theta_l(0) = s\overline{\theta}_l$, and $L(d\theta_s/dt) = s\overline{\theta_s} - \theta_s(0) = s\overline{\theta}_s$, we obtain

$$(s+A+B)\cdot\overline{\theta}_l = B\cdot\overline{\theta}_s + \frac{A-C}{s} \tag{A.7}$$

$$(s+D+F)\cdot\overline{\theta}_s = D\cdot\overline{\theta}_l + \frac{E-G}{s} \tag{A.8}$$

where $s$ is the complex argument of *Laplace* transform. Eq. (A.7) $\times (s+D+F)$ + Eq. (A.8) $\times B$:

$$[(s+A+B)(s+D+F) - BD]\cdot\overline{\theta}_l = A - C + \frac{(A-C)(D+F)+B(E-G)}{s} \tag{A.9}$$

Solve for $\overline{\theta}_l$ from Eq. (A.9), yielding

$$\overline{\theta}_l = \frac{(D+F)(A-C)+B(E-G)}{s[s^2+(A+B+D+F)s+(A(D+F)+BF)]} + \frac{A-C}{s^2+(A+B+D+F)s+(A(D+F)+BF)} \tag{A.10}$$

Eq. (A.10) can be re-written in a simpler form:

$$\overline{\theta}_l = \frac{k_1}{s(s+s_1)(s+s_2)} + \frac{k_2}{(s+s_1)(s+s_2)} \tag{A.11}$$

Eq. (A.11) is decomposed as

$$\overline{\theta}_l = \frac{k_1}{s_1\cdot s_2\cdot s} + \frac{1}{(s_1-s_2)}\cdot\left(\frac{k_1}{s_1}-k_2\right)\cdot\frac{1}{s+s_1} - \frac{1}{(s_1-s_2)}\cdot\left(\frac{k_1}{s_2}-k_2\right)\cdot\frac{1}{s+s_2} \tag{A.12}$$

Inverse *Laplace* transformation of Eq. (A.12), yielding

$$\theta_l = f_0 + f_1\cdot\exp(-s_1\cdot t) - f_2\cdot\exp(-s_2\cdot t) \tag{A.13}$$

In Eq. (A.13), the constants $f_0$, $f_1$, $f_2$, $s_1$ and $s_2$ are determined by the following definitions:

$$\xi_1 = A+B+D+F = \frac{\Delta H_i k_i}{C_{pl}\rho_l} + \frac{h_l A_s}{C_{pl}\rho_l V_l} + \frac{2h_l A_s}{C_{ps}\rho_s V_s} + \frac{2\lambda_s A_s}{L_s C_{ps}\rho_s V_s} \tag{A.14}$$

$$\xi_2 = A(D+F)+BF = \frac{\Delta H_i k_i}{C_{pl}\rho_l}\frac{2h_l A_s}{C_{ps}\rho_s V_s}\left(1+\frac{\lambda_s}{L_s h_l}\right) + \frac{h_l A_s}{C_{pl}\rho_l V_l}\cdot\frac{2\lambda_s A_s}{L_s C_{ps}\rho_s V_s} \tag{A.15}$$

$$s_1 = \frac{\xi_1 + \sqrt{\xi_1^2 - 4\xi_2}}{2} \tag{A.16}$$

$$s_2 = \frac{\xi_1 - \sqrt{\xi_1^2 - 4\xi_2}}{2} \tag{A.17}$$

$$k_1 = (D+F)(A-C)+B(E-G) = \frac{2h_l A_s}{C_{ps}\rho_s V_s}\left[\frac{\Delta H_i A_s k_i}{C_{pl}\rho_l}\left(1+\frac{\lambda_s}{L_s K_{ls}}\right) - \frac{\lambda_s A_s}{L_s C_{pl}\rho_l V_l}\cdot\frac{T_{l0}-T_c}{T_f - T_{l0}}\right] \tag{A.18}$$

$$k_2 = A - C = \frac{\Delta H_i k_i}{C_{pl}\rho_l} - \frac{h_l\cdot A_s}{C_{pl}\rho_l V_l}\cdot\frac{T_{l0}-T_{s0}}{T_f - T_{l0}} \tag{A.19}$$

$$f_0 = 1 - \frac{\frac{C}{A}+\frac{B}{A}\left(1+\frac{G}{F}\right)}{1+\frac{D}{F}+\frac{B}{A}} = 1 - \frac{T_f - T_c}{T_f - T_{l0}}\cdot\frac{1}{1+\left(1+\frac{L_s h_l}{\lambda_s}\right)\cdot\frac{\Delta H_i V_l k_i}{h_l A_s}} = 1 - \left[\frac{T_f - T_{l0}}{T_f - T_c} + \frac{\Delta H_i V_l k_i (T_f - T_{l0})}{K_{ls} A_s (T_f - T_c)}\right]^{-1} \tag{A.20}$$

where

$$\frac{1}{K_{ls}} = \frac{1}{h_l} + \frac{L_s}{\lambda_s} \tag{A.21}$$

$$f_1 = \frac{1}{s_1 - s_2}\left(\frac{k_1}{s_1} - k_2\right) = \frac{1}{s_1 - s_2}\cdot(f_0\cdot s_2 - k_2) \tag{A.22}$$

$$f_2 = \frac{1}{s_1 - s_2}\left(\frac{k_1}{s_2} - k_2\right) = \frac{1}{s_1 - s_2}\cdot(f_0\cdot s_1 - k_2) \tag{A.23}$$

## References


[1] P.A. Intemann, M. Kazmierczak, Heat transfer and ice formations deposited upon cold tube bundles immersed in flowing water. I. Convection analysis, Int. J. Heat Mass Transfer 40 (3) (1997) 557–572.

[2] M. Kazmierczak, P.A. Intemann, Heat transfer and ice formations deposited upon cold tube bundles immersed in flowing water. II. Conjugate analysis, Int. J. Heat Mass Transfer 40 (3) (1997) 573–588.

[3] D. Tsuchida et al., Ice formation process by cooling water–oil emulsion with stirring in a vessel, Int. J. Refrigerat. 25 (2002) 250–258.

[4] V.J. Lunardini, Heat Transfer with Freezing and Thawing, Elsevier Science Publ. Co, Amsterdam, 1991, p. 41.

[5] K.A. Fikiin, Generalized numerical modelling of unsteady heat transfer during cooling and freezing using an improved enthalpy method and quasi-one-dimensional formulation, Int. J. Refrigerat. 19 (2) (1996) 132–144.

[6] W.-Q. Lu, Boundary element analysis of the heat transfer in Bridgman growth process of semi-transparent crystals, Mater. Sci. Eng. A 292 (2000) 219–223.

[7] G. Comini, O. Saro, Numerical modelling of freezing processes in foodstuffs, in: Computational modelling of free and moving boundary problems: Proceedings of the First International Conference, Computational Mechanics Publications, Southampton, UK, 1991, pp. 27–37.
[8] H. Garabedian, R.F. Strickland-Constable, Collision breeding of ice crystals, J. Cryst. Growth 22 (1974) 188.
[9] J.-S. Wey, J. Estrin, Modeling the batch crystallization process. The ice–brine system, Ind. Eng. Chem. Process Design Develop. 12 (1973) 237.
[10] A. Mersmann (Ed.), Crystallization Technology Handbook, Marcel Dekker Inc., New York, 1995, pp. 314–316.
[11] S.G. Kane, Secondary nucleation of ice in a stirred batch crystallizer, SC.D. Thesis, Mass. Inst. Technol., Cambridge, 1971.
[12] S.G. Kane, T.W. Evans, P.L.T. Brian, A.F. Sarofem, Determination of the kinetics of secondary nucleation in batch crystallizers, AIChE J. 20 (5) (1974) 855–862.
[13] A.M. Omran, C.J. King, Kinetics of ice crystallization in sugar solution and fruit juices, AIChE Journal 20 (4) (1974) 795–802.
[14] J.H. Stocking, C.J. King, Secondary nucleation of ice in sugar solutions and fruit juices, AIChE J. 22 (1) (1976) 131–140.
[15] Y. Shirai, K. Nakanishi, R. Matsuno, T. Kamikubo, On the kinetics of ice crystallization in batch crystallizers, AIChE J. 31 (4) (1985) 676–682.
[16] Y. Shirai, K. Nakanishi, R. Matsuno, T. Kamikubo, Effects of polymers on secondary nucleation of ice crystals, J. Food Sci. 50 (1985) 401–406.
[17] X.D. Chen, P. Chen, K.W. Free, Experimental data on the time-to-onset of ice formation at the metal surface correlated using a sub-layer reactor model, Int. J. Heat Mass Transfer 43 (1999) 643–652.
[18] P.N.V. Tu, Dynamical Systems: An Introduction with Applications in Economics and Biology, second ed., Springer-Verlag, Berlin, 1994, p. 314.
[19] R.J.C. Vaessen, C. Himawan, G.J. Witkamp, Scale formation of ice from electrolyte solutions on a scraped surface heat exchanger plate, J. Cryst. Growth 237–239 (April) (2002) 2172–2177.
[20] P. Chen, Freeze concentration of food liquids using layer crystallizers, Ph.D. Thesis, Department of Chemical and Materials Engineering, The University of Auckland, Auckland, 1999.
[21] F.G.F. Qin, A.B. Russell, X.D. Chen, Experimental study of ice fouling on the subcooled metal surfaces, in: 9th Asian Pacific Confederation of Chemical Engineering (APCChE) and 30th Annual Australasian Chemical Engineering Conference (CHEMECA), 29 September–3 October 2002, University of Canterbury, Christchurch, New Zealand.
[22] W.L. McCabe, J.C. Smith, P. Harriott, Unit Operations of Chemical Engineering, McGraw-Hill Inc., New York, 1993.
[23] B.H. Webb, A.H. Johnson, J.A. Alford (Eds.), Fundamentals of Dairy Chemistry, second ed., The Avi Publishing Company Inc, Westport, Connecticut, 1978, p. 413.
[24] R.K. Robinson (Ed.), Modern Dairy Technology, second ed., vol. 2, Elsevier Applied Science, London and New York, 1993, p. 349.